Probing the non-Debye low-frequency excitations in glasses through random pinning

Luca Angelani[a,b], Matteo Paoluzzi[c], Giorgio Parisi[b,d,e,1], and Giancarlo Ruocco[b,f]

[a]Institute for Complex Systems, National Research Council (ISC-CNR), 00185 Rome, Italy; [b]Dipartimento di Fisica, Sapienza Università di Roma, 00185 Rome, Italy; [c]Department of Physics, Syracuse Soft & Living Matter Program, Syracuse University, Syracuse NY 13244; [d]Nanotec, CNR, 00185 Rome, Italy; [e]Istituto Nazionale di Fisica Nucleare (INFN) Sezione di Roma I, 00185 Rome, Italy; and [f]Center for Life NanoScience, Istituto Italiano di Tecnologia, 00161 Rome, Italy

Contributed by Giorgio Parisi, July 12, 2018 (sent for review March 22, 2018; reviewed by Jeppe C. Dyre and Walter Kob)

We investigate the properties of the low-frequency spectrum in the density of states $D(\omega)$ of a 3D model glass former. To magnify the non-Debye sector of the spectrum, we introduce a random pinning field that freezes a finite particle fraction to break the translational invariance and shifts all of the vibrational frequencies of the extended modes toward higher frequencies. We show that non-Debye soft localized modes progressively emerge as the fraction p of pinned particles increases. Moreover, the low-frequency tail of $D(\omega)$ goes to zero as a power law $\omega^{\delta(p)}$, with $2 \leq \delta(p) \leq 4$ and $\delta = 4$ above a threshold fraction p_{th}.

inherent structures | low temperature | energy spectrum | glasses | non-Debye law

Understanding the peculiarities and the universal features of the low-frequency spectrum in glasses plays a crucial role to gain insight into their thermal and mechanical properties.

In the case of crystalline solids, mechanical and thermal properties follow universal laws that can be obtained through Debye's theory. Debye's law assumes that the only energy excitations around the ground state in crystals are phonons, that is, Goldstone modes. The corresponding density of states $D(\omega)$ below Debye's frequency follows $D(\omega) \sim \omega^{d-1}$, in d spatial dimensions (1).

More complex is the situation for amorphous systems where the low-frequency spectrum shows an abundance of soft non-Goldstone modes. Quasi-localized soft modes are involved, for example, in the relaxation processes of a supercooled liquid (2) and in the plastic flow of disordered solids (3). They have a natural interpretation within the jamming transition (4, 5) due to a class of exactly solvable mean-field models (6–8).

Theoretical models of random media predict a universal law for the density of states of the non-Goldstone (i.e. nonphononic) component of the spectrum with a scaling $D(\omega) \sim \omega^4$ in any dimensions (9, 10). Experiments suggested this behavior in real glasses (11) and, consistently, it was recently shown that in many real and simulated glasses the non-Debye contribution to the density of states is proportional to the phonon damping, thus showing the well-known Rayleigh fourth power frequency dependence (11–15).

However, since on a large enough scale glasses are continuum media, the phononic contribution in $D(\omega)$ dramatically overcomes any subdominant non-Goldstone tail at low frequencies (13). Numerical simulations of a repulsive binary mixture suggest that the Goldstone modes hybridize with non-Goldstone excitations and destroy the ω^4 tail (16).

The coexistence of phonons and soft-localized modes requires one to separate the two contributions for studying the low-frequency spectrum (17). In particular, to probe the non-Goldstone modes, one needs a protocol to cancel the Goldstone modes from the low-frequency region by choosing suitably small systems (18). Recently, it has been possible to observe a non-Goldstone low-frequency sector of the spectrum in the density of states of structural glasses and disordered systems that follows a power law $D(\omega) \sim \omega^4$ (17–21).

In this paper, in analogy with the procedure adopted in ref. 19 where a random field was introduced in the Heisenberg spin glass to destroy the spin-wave contribution at low frequencies, we use a random pinning field that freezes a finite fraction of particles. The presence of this random external field destroys any spatial symmetry, removing the corresponding Goldstone excitations (22).

Random pinning has been largely used to gain more information about random–first-order theory in glass-forming liquids (23–33). In the following, we show that random pinning allows us also to improve our knowledge about the density of states in amorphous solids.

Here, we perform molecular dynamics simulations of a particulate glass model in 3D. After equilibrating the fluid at high temperatures, we compute the density of states obtained through the normal modes around the corresponding inherent structures. In computing the inherent structures, we freeze a particle fraction p. The snapshots of two minimized configurations with different fractions of pinned particles are shown in Fig. 1. By progressively increasing p, we observe that the resulting low-frequency spectrum qualitatively changes. In particular, it develops a non-Debye tail. We find that the low-frequency spectrum is populated by soft modes that reach zero as a power law $D(\omega) \sim \omega^{\delta}$. The exponent δ departs continuously from the Debye value $\delta = 2$ that is recovered at a small fraction of pinned particles. For large p values, the exponent approaches the limit value $\delta = 4$. Moreover, the non-Goldstone modes become progressively quasi-localized as the number of frozen particles increases.

Results

As a model glass former, we consider a binary mixture $50:50$ composed of a soft sphere in 3D. The particles interact with each

Significance

Amorphous solids are continuum media. However, their mechanical and thermodynamical properties, even though universal, dramatically deviate from those in crystalline solids. Their anomalous behavior reflects peculiar and universal deviations from Debye's law in the low-frequency sector of the density of states $D(\omega)$. Theoretical models predict a population of non-Goldstone modes following the universal power law $D(\omega) \sim \omega^4$ that are subdominant and therefore hard to detect. In this work, we introduce a general protocol that can be used in both numerical simulations and experiments, to probe the non-Debye portion of the spectrum.

Author contributions: G.P. conceived research; L.A., M.P., G.P., and G.R. designed research; M.P. and G.R. performed research; and M.P. wrote the paper.

Reviewers: J.C.D., Roskilde University; and W.K., University of Montpellier.

The authors declare no conflict of interest.

[1]To whom correspondence should be addressed. Email: giorgio.parisi@roma1.infn.it.

Published online August 13, 2018.

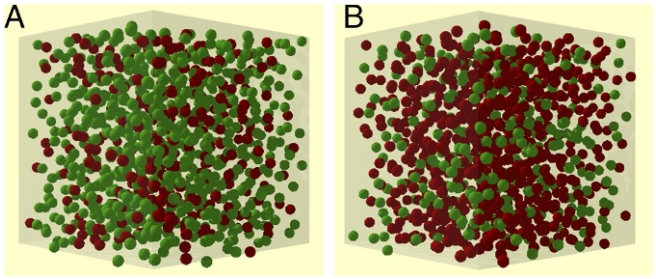

Fig. 1. (*A* and *B*) Snapshots of inherent structures with $p = 0.3$ (*A*) and $p = 0.7$ (*B*). Red particles are frozen during the minimization of the energy.

other through an r^{-12} potential. The details about the model and numerical simulations are given in *Materials and Methods*. The typical protocol adopted for investigating the vibrational modes is the following. We start with thermalizing a configuration at a high temperature far above the dynamical temperature T_{MC} of the model, that is, the temperature where the system undergoes a dynamical arrest. In our simulations, the dynamical temperature results to be $T_{MC} \sim 0.2$. We study glassy states obtained by instantaneous quenching configurations equilibrated at high temperature $T = 3\,T_{MC}$, that is, deep in the liquid state. The inherent structure of the equilibrated configuration is then computed by minimizing the mechanical energy. In computing the inherent structure, we randomly choose a finite fraction p of particles that is maintained frozen during energy minimization. The vibrational modes are obtained through the diagonalization of the corresponding dynamical matrix.

We start our discussion by considering a system composed of $N = 1{,}000$ particles. Fig. 2*A* shows the cumulative distribution of the density of states $F(\omega)$ (*Materials and Methods*). This quantity shows a power-law tail at low frequency, $F(\omega) \sim \omega^{\alpha}$, corresponding to a power-law tail of the density of states, $D(\omega) \sim \omega^{\delta} = \omega^{\alpha-1}$. For $p = 0$, the Debye contribution dominates the low-frequency spectrum below the Boson peak. In that region, the cumulative distribution reaches zero as $F(\omega) \sim \omega^3$; that is, $\alpha = d$. By increasing the fraction of pinned particles p, we observe a progressive disappearance of the Goldstone modes in favor of non-Goldstone modes. The dashed curves are the fit to the power law ω^{α}, and we obtain a monotonic growing of α with increasing p that eventually saturates at the value $\alpha = 5$. The behavior of $\alpha - 1$ as a function of p is shown in Fig. 2*B*. To give an estimate for the crossover between the Debye and the non-Debye regime, we fit the curve $\delta(p) = \alpha(p) - 1$ to a generalized logistic curve $\delta(p) = \delta_{min} + \frac{\delta_{min} - \delta_{max}}{1 + e^{\frac{p - p_{th}}{\sigma}}}$, where $\delta_{min} = 2$, $\delta_{max} = 4$, and p_{th} and σ are the fitting parameters. The parameter p_{th} gives an estimate for the threshold values of p between the two regimes. The logistic curve provides a good fit to the data with $p_{th} = 0.47 \pm 0.01$ (black dashed line in Fig. 2*B*). To be sure that random pinning does not dramatically alter the structural properties of the glass, we kept track of the radial distribution function $g(r)$ of the configuration that minimizes the energy. As shown in Fig. 2*C*, where we plot the evolution of $g(r)$ for different values of p, random pinning does not alter the structure of the system that remains amorphous even at a large pinned particle fraction. At a very high fraction p above p_{th}, a few moving particles are caged by a large number of nonmoving particles. In that situation, as we show later, the vibrational modes are totally localized.

In Fig. 3 we show $D(\omega)$ for $N = 1{,}000$ particles and $p = 0, 0.3, 0.6$. Red and green dashed lines in Fig. 3*A* are the power laws ω^2 and ω^4, respectively. The two scaling regimes are made more clear in Fig. 3 *B* and *C*, where $D(\omega)/\omega^2$ and $D(\omega)/\omega^4$ for $p = 0.0, 0.6$ are shown. The dashed lines are a guide to the eye that indicate $D(\omega)/\omega^{\delta} = const$. Here, we are focusing our attention on non-Debye modes in the low-frequency spectrum. However, as is well known in the study of structural glasses, extended modes are responsible for the excess modes with respect to the Debye density of states at intermediate frequencies also called the Boson peak (34, 35). The presence of the Boson peak in the model considered here is made clear in Fig. 3*B*, *Inset* where $D(\omega)/\omega^2$ is plotted in semilog scale. The red arrow indicates the position of the peak for $p = 0$. As one can see, the random pinning besides destroying the Debye scaling attenuates the peak that shifts at higher frequencies. Since the presence of the Boson peak is due to extended modes, the attenuation of the peak with increasing the number of frozen particles is consistent with the suppression of extended modes in favor of localized ones.

To gain access to lower frequencies, we perform simulations up to $N = 8{,}000$ particles. The corresponding $F(\omega)$, opportunely normalized with the total number of modes, is shown in Fig. 2*D*.

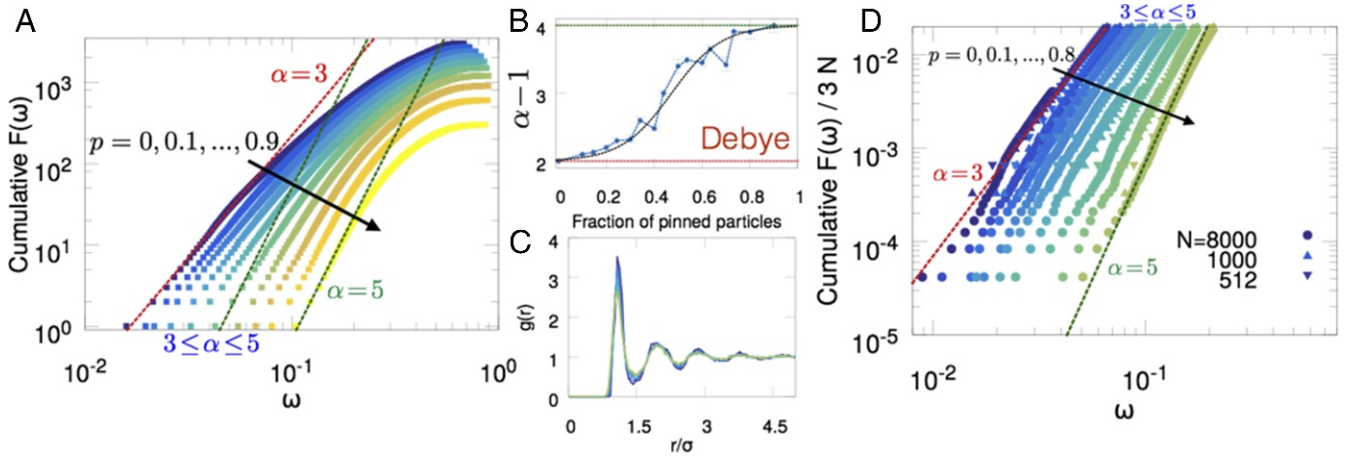

Fig. 2. (*A*) The cumulative function of the density of states $F(\omega)$ deviates progressively from Debye by increasing the fraction of pinned particles p, from 0 (blue) to 0.9 (yellow). The considered system size is $N = 1{,}000$. (*B*) From the tail of $F(\omega)$ we fit the exponent α that saturates toward 5 by increasing p. The black dashed curve is the best fit to the logistic function. (*C*) Radial distribution function at different pinned particle fractions, from $p = 0$ (blue) to $p = 0.8$ (yellow). (*D*) Normal modes from different system sizes $N = 512$, 1,000, 8,000 smoothly connect with each other. The red dashed line and the green dashed line are a guide to the eye for $F(\omega) \sim \omega^3$ and $F(\omega) \sim \omega^5$, respectively.

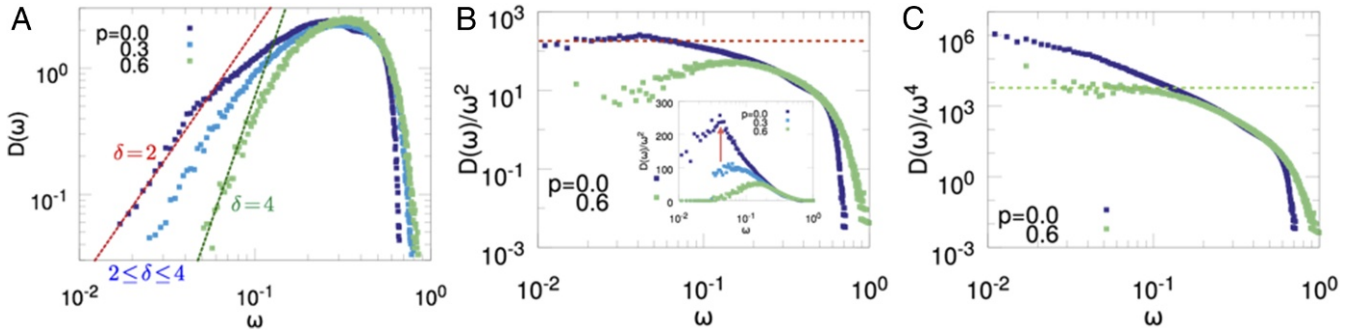

Fig. 3. (*A*) The density of states $D(\omega)$ for $N = 1{,}000$ particles at $p = 0$ (blue), 0.3 (light-blue), and 0.6 (green). The red dashed curve is the Debye scaling $\sim\omega^2$. The green dashed curve indicates $D(\omega) \sim \omega^4$. Debye and non-Debye spectra are highlighted in *B* and *C*, where we plot $D(\omega)/\omega^2$ and $D(\omega)/\omega^4$, respectively. *B*, *Inset* shows $D(\omega)/\omega^2$ in semilog scale, and the Boson peak at $p = 0$ is indicated by the red arrow.

As we can appreciate, normal modes from $N = 512, 1{,}000, 8{,}000$ smoothly connect with each other and the corresponding tail connects continuously with no gap. Again, the exponent of the power law $F(\omega) \sim \omega^{\alpha}$ depends on p and interpolates between Debye $\alpha = 3$ and non-Debye $\alpha = 5$ as the fraction of frozen particles increases. This finding proves that the low-frequency spectrum probed at the smallest size $N = 512$ is representative also for larger system sizes.

Soft modes in glasses are local excitations responsible for the plastic flow (36–38). Localization can be quantified through the inverse participation ratio $IPR(\omega)$ (39, 40). The details about its computation are given in *Materials and Methods*. Delocalized modes cover the entire system and $IPR(\omega) \to 1/N$. Fully localized modes involve few particles, meaning that the corresponding eigenvectors count few components. Localization is then signaled by a scaling $IPR(\omega) \sim 1$. The $IPR(\omega)$ computed for $N = 1{,}000$ particles is shown in Fig. 4*A*. When $p = 0$, phonons dominate the spectrum, they are extended excitations, and consequently $IPR \sim 10^{-3} = N^{-1}$. With increasing the fraction of pinned particles, $IPR(\omega)$ increases too. Moreover, localization involves particularly the lowest-frequency modes. This is the signal where modes populating the non-Goldstone sector of $D(\omega)$ are progressively quasi-localized in few particle sites. To better quantify the localization properties of the low-frequency modes, we compute the probability distribution $P(IPR)$ to find a mode ω with an inverse participation ratio IPR (41). The distribution has been computed for modes ω falling in the portion ω^{δ} of the spectrum. As shown in Fig. 4 *C* and *F*, the distribution develops a peak which drifts to high *IPR* values upon increasing the fraction of frozen particles p, accompanied by a broadening of the distribution. Moreover, we observe long tails on the right part of the distribution at high *IPR* values (localized modes) and the appearance of a second peak at *IPR* = 1 for $p = 0.8$, indicating that, due to the cage effect generated by the increasing number of frozen particles, the modes are fully localized in a few particles.

Finally, we studied the relation between localized soft modes and pinned particles. For each frozen fraction p, we computed the number of particles lying in a sphere of radius $r^* = 1.6\sigma$ centered around a given nonpinned particle. The value of r^* is chosen between the two first peaks of the radial distribution function $g(r)$. As shown in Fig. 4*B*, above the threshold value

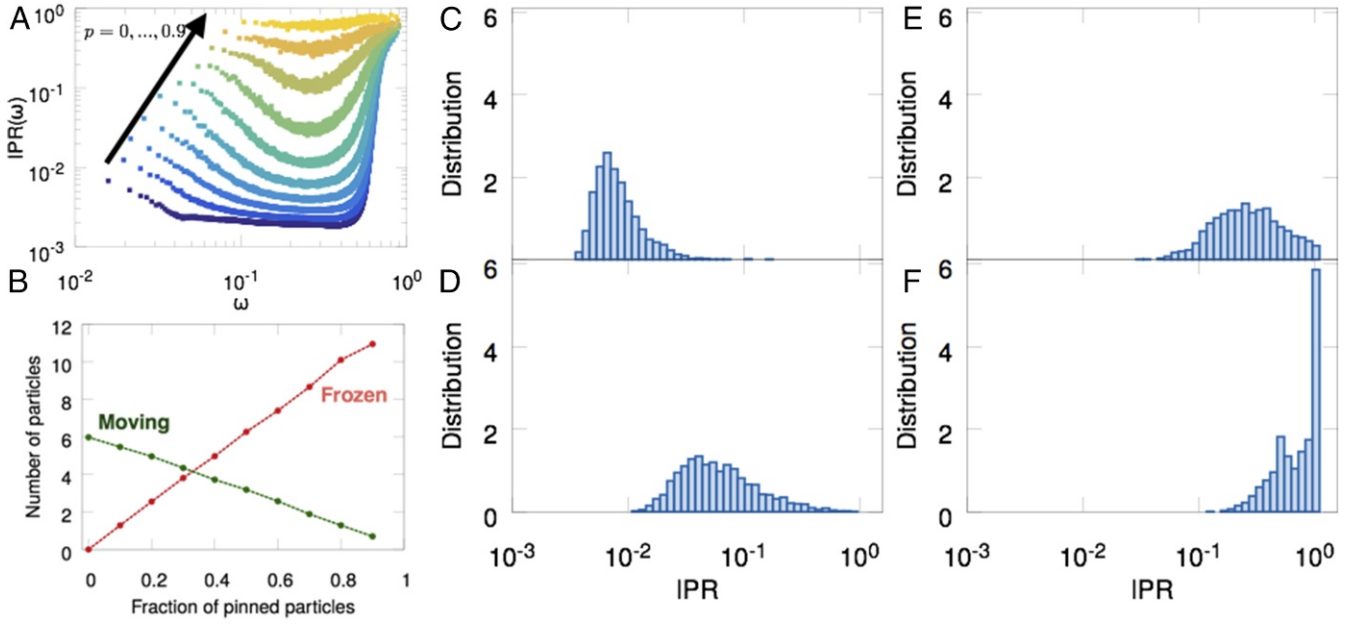

Fig. 4. (*A*) *IPR* by increasing the fraction of pinned particles from $p = 0$ (purple) to 0.9 (yellow) for a system size $N = 1{,}000$. (*B*) Number of moving (green symbols) and frozen (red symbols) particles inside a shell of radius 1.6σ. (*C*–*F*) Probability distribution of the IPR for the modes in the ω^{δ} scaling regime. The fractions of frozen particles are $p = 0.2$ (*C*), 0.5 (*D*), 0.7 (*E*), and 0.9 (*F*).

$p_{th} = 0.47$ that we estimated previously, each nonpinned particle is surrounded by a large number of pinned particles. In this way, by increasing the number of frozen particles, we are progressively probing vibrational modes related to a few particles caged in a random environment. At the higher values of the pinning fraction p each particle is surrounded on average just by frozen particles. The resulting vibrational modes are fully localized, giving rise to the peak in the distribution $P(IPR)$ at $IPR \sim 1$.

Summary and Discussion

The anomalous thermal and mechanical properties of glasses are strongly related to their non-Debye excitations that populate the low-frequency spectrum. For this reason, it is crucial to develop techniques and protocols that allow us to efficiently probe the subdominant glassy modes.

In this paper, we investigated the low-frequency spectrum of a colloidal glass in 3D. To gain insight into the non-Debye sector of $D(\omega)$, we use the random pinning protocol that randomly freezes a particle fraction. We show that the random pinning procedure progressively destroys any spatial symmetry present in the system, removing the phononic contribution to $D(\omega)$. In particular, the suppression of phonons by increasing the fraction of frozen particles attenuates the Boson peak and magnifies the presence of soft localized glassy modes.

We have also shown that non-Goldstone modes progressively emerge in the spectrum as the fraction of frozen particles increases. Moreover, the power law in the tail of $D(\omega) \sim \omega^{\delta}$ smoothly changes from Debye, that is, $\delta = 2$, to $\delta = 4$ at a high pinning fraction. The power law $D(\omega) \sim \omega^4$ is fully consistent with the theoretical prediction for Bosonic non-Goldstone excitations given in ref. 10 that has been also confirmed recently in numerical simulations (17–19) and in the analysis of the sound attenuation in real and simulated glasses (12). We also found that the low-frequency sector is populated by soft modes that become progressively localized in few particle sites. At large pinned particle fractions, the moving particles are caged by the nonmoving ones and the corresponding vibrational modes are extremely localized. It is worth noting that, even in that extreme situation, the density of states follows the ω^4 scaling law.

It is worth noting that the scenario here proposed, that is, the coexistence at low frequency of propagating/extended phononic modes with non-Goldstone/localized states, is consistent with the recently developed "heterogeneous viscoelasticity" theory (42) where the role of pinning (or of the "external field") is played by the presence of regions with higher elastic moduli in the glass.

As a concluding remark, our study suggests an alternative way to probe the properties of plastic modes in glassy and disordered materials in both numerical simulations and experiments.

In computer simulations, the protocol considered here has an advantage that works at any system sizes for the repulsive potentials, that is, colloidal glasses. This suggests that, for instance, it is not necessary to tune the system size below a threshold value as in ref. 18 or perform large-scale simulations to approach the continuum limit (17). Since numerical studies on low-frequency localized modes in glasses are usually focused on colloidal glasses obtained by considering repulsive pairwise potentials (16, 17, 21), as a future direction, it would be interesting to study the case of an attractive potential such as in a Kob–Andersen binary mixture (43) to understand whether and how attraction modifies the non-Goldstone spectrum in structural glasses.

As a final remark, random pinning fields able to trap many colloids through a single laser beam can be generated in a laboratory by means of speckle patterns (44) or by means of suitable algorithms for the control of the spatial light modulator to obtain multifocus beams (45). In that way, it is possible to isolate the non-Goldstone contribution in the low-frequency vibrational modes that are accessible in colloidal glasses by means of confocal microscopy (46).

Materials and Methods

Model. As glass-forming model, we consider a 50 : 50 binary mixture of large and small soft spheres in 3D (47). Indicating with $\mathbf{r}_i$ the position of the particle i, with $i = 1, \ldots, N$, two particles i, j interact via a pure repulsive potential $\phi(r_{ij})$, where $r_{ij} \equiv |\mathbf{r}_i - \mathbf{r}_j|$. The potential reads

$$\phi(r_{ij}) = \left(\frac{\sigma_i + \sigma_j}{r_{ij}} \right)^{12} + \alpha + \beta r_{ij}^2, \qquad [1]$$

where σ_i takes the value σ_A for the large particles and σ_B for the small ones, with $\sigma_A/\sigma_B = 1.2$ and $\sigma_A + \sigma_B \equiv \sigma = 1$. We consider $N = N_A + N_B$ particles ($N_A = N_B$) that are enclosed in a 3D box of side $L = \sigma N^{1/3}$ where periodic boundary conditions are used. The expression for L guarantees $\rho = N/V = 1$, with ρ the particle density. Moreover, we impose a cutoff to the potential ϕ at $r_c = 1.5\sigma$ in a way that $\phi(r) = 0$ for $r > r_c$. The coefficients α and β are chosen to ensure the continuity of $\phi(r)$ up to the first derivative at $r = r_c$.

In the following we report all quantities in reduced units. The molecular dynamics simulations are performed in the *NVT* ensemble at temperature $T = 3\,T_{MC}$, where T_{MC} is the mode-coupling temperature of the model, that is, defined according to $\tau_\alpha(T) \sim (T - T_{MC})^{-\gamma}$, with τ_α the timescale of the α processes. We also performed swap Monte Carlo simulations in the *NVT* ensemble. In that case, the thermalization of the fluid is controlled by looking at the evolution of the total potential energy $\Phi(\{\mathbf{r}_i\}) = \sum_{i<j} \phi(r_{ij})$ as a function of temperature and comparing it with the Rosenfeld and Tarazona formula $A + BT^{3/5}$ (48). The system sizes are $N = 512$, 1,000, 1,024, 8,000.

Inherent Structures and Vibrational Mode Analysis. After thermalization, we compute the corresponding inherent structures that are obtained by minimizing the configurational energy $\Phi(\{\mathbf{r}_i\})$. During the energy minimization, we consider a finite particle fraction pN, with $p \in [0, 1[$, frozen in its equilibrium configuration.

To compute the density of states, we expand Φ around the configuration $\{\mathbf{r}_i^0\}$ that minimizes the energy

$$\Phi(\{\mathbf{r}_i\}) = \Phi(\{\mathbf{r}_i^0\}) + \frac{1}{2} \sum_{i,\alpha j,\beta} \delta r_i^\alpha \, \mathcal{H}_{i\alpha j\beta} \, \delta r_j^\beta + \ldots, \qquad [2]$$

where $\delta r_i^\alpha \equiv r_i^\alpha - r_i^{\alpha,0}$ and we consider only the nonpinned particles. In Eq. **2**, we defined the dynamical matrix

$$\mathcal{H}_{i\alpha j\beta} \equiv \left. \frac{\partial^2 \phi(r_{ij})}{\partial r_i^\alpha \partial r_j^\beta} \right|_{\{\mathbf{r}_i^0\}}, \qquad [3]$$

where the Latin indexes $i, j = 1, \ldots, N$ indicate the particles and Greek symbols $\alpha, \beta = 1, \ldots, d$ are the Cartesian coordinates.

The energy minimization was obtained through the limited-memory Broyden–Fletcher–Goldfarb–Shanno algorithm (49). For each value of p, we collected data for 10^2 inherent structures obtained by considering a different thermalized configuration. At the end of the minimization, we checked the structural properties of the corresponding configuration through the radial distribution function

$$g(r) = \frac{V}{4\pi r^2 N^2} \left\langle \sum_i \sum_{j \neq i} \delta(r - |\mathbf{r}_i - \mathbf{r}_j|) \right\rangle, \qquad [4]$$

where the angle brackets denote the average over 10^2 independent configurations and $\delta(x)$ is the Dirac delta function.

The normal modes are then obtained through the diagonalization of the dynamical matrix $\mathcal{H}$. For system sizes up to 1,024, we evaluate the entire eigenvalue spectrum through gsl-GNU libraries, and for larger sizes we compute the lowest 100 eigenvalues with ARPACK (50). Indicating with λ_κ the eigenvalues of $\mathcal{H}$, the corresponding $3N$ squared normal-mode frequencies are $\omega_\kappa^2 = \lambda_\kappa$. From the spectrum of the eigenvalues $\rho(\lambda)$, using the relation between ω_κ and λ_κ, we compute both the cumulative function $F(\omega)$ and the density of states $D(\omega)$; that is,

$$D(\omega) = \frac{1}{\mathcal{N}} \sum_{m=1}^{\mathcal{N}} \delta(\omega - \omega_m), \quad [5]$$

where $\mathcal{N}$ is the number of nonzero modes. When $p = 0$, one has $\mathcal{N} = 3N - 3$ since we have to remove the three zero modes responsible for translational invariance. When $p > 0$, translational invariance is naturally broken and the number of modes is $\mathcal{N} = 3(1 - p)N$. The cumulative function $F(\omega)$ reads

$$F(\omega) = \int_0^{\omega} d\omega' \, D(\omega') \, . \quad [6]$$

In the case of a 3D elastic solid, the spectrum at low frequencies is populated by phonons; that brings to the power law $F(\omega) \sim \omega^d$ and $D(\omega) \sim \omega^{d-1}$. If the low-frequency spectrum is populated by non-Goldstone soft modes, one expects that $D(\omega)$ reaches zero as a power law with $D(\omega) \sim \omega^{\delta}$ and, consequently, $F(\omega) \sim \omega^{\alpha}$, with $\alpha - 1 = \delta$.

As a measure of the spatial extension of the normal modes, we compute the inverse participation ratio $IPR(\omega)$ defined as (40)

$$IPR(\omega) \equiv \frac{\sum_i |\mathbf{e}_i(\omega)|^4}{(\sum_i |\mathbf{e}_i(\omega)|^2)^2}, \quad [7]$$

where $\mathbf{e}_i(\omega)$ is the eigenvector of the mode ω. For a completely localized mode ω on a single particle, one has $IPR(\omega) = 1$, while a mode extended over all of the particles corresponds to $IPR(\omega) \sim N^{-1}$.

Finally, we computed the probability distribution function of the inverse of the participation ratio for quasi-localized modes $P(IPR)$, that is, the probability to find a mode ω with inverse of participation ratio IPR; that is,

$$P(IPR) = \Omega^{-1} \left\langle \sum_{m<max} \delta \left[IPR - IPR(\omega_m) \right] \right\rangle, \quad [8]$$

where the normalization Ω^{-1} guarantees $\int d[IPR] \, P(IPR) = 1$. The distribution was obtained by considering normal modes $\omega_m < \omega_{max}$ in the power-law region, that is, where the density of states follows the ω^{δ} scaling.

ACKNOWLEDGMENTS. M.P. was supported by a Simons Foundation Targeted Grant in the Mathematical Modeling of Living Systems (Grant 342354) and by the Syracuse Soft & Living Matter Program. G.P. acknowledges the financial support of the Simons Foundation (Grant 454949). This project received funding from the European Research Council under the European Union's Horizon 2020 research and innovation programme (Grant 694925).

1. Kittel C (2005) *Introduction to Solid State Physics* (John Wiley and Sons, New York), 7th Ed.
2. Widmer-Cooper A, Perry H, Harrowell P, Reichman DR (2008) Irreversible reorganization in a supercooled liquid originates from localized soft modes. *Nat Phys* 4:711–715.
3. Manning ML, Liu AJ (2011) Vibrational modes identify soft spots in a sheared disordered packing. *Phys Rev Lett* 107:108302.
4. O'Hern CS, Silbert LE, Liu AJ, Nagel SR (2003) Jamming at zero temperature and zero applied stress: The epitome of disorder. *Phys Rev E* 68:011306.
5. Wyart M (2012) Marginal stability constrain force and pair distributions at random close packing. *Phys Rev Lett* 109:125502.
6. Franz S, Parisi G, Urbani P, Zamponi F (2015) Universal spectrum of normal modes in low-temperature glasses. *Proc Natl Acad Sci USA* 112:14539–14544.
7. Kurchan J, Parisi G, Urbani P, Zamponi F (2013) Exact theory of dense amorphous hard spheres in high dimension. II. The high density regime and the Gardner transition. *J Phys Chem B* 117:12979–12994.
8. Charbonneau P, Kurchan J, Parisi G, Urbani P, Zamponi F (2017) Glass and jamming transitions: From exact results to finite-dimensional descriptions. *Annu Rev Condens Matter Phys* 8:265–288.
9. Gurarie V, Chalker JT (2003) Bosonic excitations in random media. *Phys Rev B* 68:134207.
10. Gurevich VL, Parshin DA, Schober HR (2003) Anharmonicity, vibrational instability, and the boson peak in glasses. *Phys Rev B* 67:094203.
11. Gelin S, Tanaka H, Lemaître A (2016) Anomalous phonon scattering and elastic correlations in amorphous solids. *Nat Mater* 15:1177–1181.
12. Schirmacher W, Ruocco G, Scopigno T (2007) Acoustic attenuation in glasses and its relation with the Boson Peak. *Phys Rev Lett* 98:025501.
13. Shintani H, Tanaka H (2008) Universal link between the boson peak and transverse phonons in glass. *Nat Mater* 7:870–877.
14. Rufflé B, Foret M, Courtens E, Vacher R, Monaco G (2003) Observation of the onset of strong scattering on high frequency acoustic phonons in densified silica glass. *Phys Rev Lett* 90:095502.
15. Rufflé B, Guimbretière G, Courtens E, Vacher R, Monaco G (2006) Glass-specific behavior in the damping of acousticlike vibrations. *Phys Rev Lett* 96:045502.
16. Lerner E, Gartner L (2016) Nonlinear modes disentangle glassy and goldstone modes in structural glasses. *SciPost Phys* 1:016.
17. Mizuno H, Shiba H, Ikeda A (2017) Continuum limit of the vibrational properties of amorphous solids. *Proc Natl Acad Sci USA* 114:E9767–E9774.
18. Lerner E, Düring G, Bouchbinder E (2016) Statistics and properties of low-frequency vibrational modes in structural glasses. *Phys Rev Lett* 117:035501.
19. Baity-Jesi M, Martín-Mayor V, Parisi G, Perez-Gaviro S (2015) Soft modes, localization, and two-level systems in spin glasses. *Phys Rev Lett* 115:267205.
20. Lerner E, Bouchbinder E (2017) Effect of instantaneous and continuous quenches on the density of vibrational modes in model glasses. *Phys Rev E* 96:020104.
21. Lerner E, Düring G, Bouchbinder E (2016) Statistics and properties of low-frequency vibrational modes in structural glasses. *Phys Rev Lett* 117:035501.
22. Lupo C (2017) Critical properties of disordered xy model on sparse random graphs. arXiv:1706.08899.
23. Kob W, Roldán-Vargas S, Berthier L (2012) Non-monotonic temperature evolution of dynamic correlations in glass-forming liquids. *Nat Phys* 8:164–167.
24. Cammarota C, Biroli G (2012) Ideal glass transitions by random pinning. *Proc Natl Acad Sci USA* 109:8850–8855.
25. Ozawa M, Kob W, Ikeda A, Miyazaki K (2015) Equilibrium phase diagram of a randomly pinned glass-former. *Proc Natl Acad Sci USA* 112:6914–6919.
26. Kob W, Berthier L (2013) Probing a liquid to glass transition in equilibrium. *Phys Rev Lett* 110:245702.
27. Cammarota C, Biroli G (2013) Random pinning glass transition: Hallmarks, mean-field theory and renormalization group analysis. *J Chem Phys* 138:12A547.
28. Brito C, Parisi G, Zamponi F (2013) Jamming transition of randomly pinned systems. *Soft Matter* 9:8540–8546.
29. Gokhale S, Nagamanasa KH, Ganapathy R, Sood A (2014) Growing dynamical facilitation on approaching the random pinning colloidal glass transition. *Nat Commun* 5:4685.
30. Nagamanasa KH, Gokhale S, Sood A, Ganapathy R (2015) Direct measurements of growing amorphous order and non-monotonic dynamic correlations in a colloidal glass-former. *Nat Phys* 11:403–408.
31. Szamel G, Flenner E (2013) Glassy dynamics of partially pinned fluids: An alternative mode-coupling approach. *Europhys Lett* 101:66005.
32. Karmakar S, Parisi G (2013) Random pinning glass model. *Proc Natl Acad Sci USA* 110:2752–2757.
33. Chakrabarty S, Karmakar S, Dasgupta C (2015) Dynamics of glass forming liquids with randomly pinned particles. *Sci Rep* 5:12577.
34. Binder K, Kob W (2005) *Glassy Materials and Disordered Solids: An Introduction to Their Statistical Mechanics* (World Scientific, Singapore).
35. Buchenau U, Nücker N, Dianoux A (1984) Neutron scattering study of the low-frequency vibrations in vitreous silica. *Phys Rev Lett* 53:2316.
36. DeGiuli E, Lerner E, Brito C, Wyart M (2014) Force distribution affects vibrational properties in hard-sphere glasses. *Proc Natl Acad Sci USA* 111:17054–17059.
37. Charbonneau P, Corwin EI, Parisi G, Zamponi F (2015) Jamming criticality revealed by removing localized buckling excitations. *Phys Rev Lett* 114:125504.
38. Xu N, Vitelli V, Liu AJ, Nagel SR (2010) Anharmonic and quasi-localized vibrations in jammed solids—modes for mechanical failure. *Europhys Lett* 90:56001.
39. Mazzacurati V, Ruocco G, Sampoli M (1996) Low-frequency atomic motion in a model glass. *Europhys Lett* 34:681.
40. Bell R, Dean P (1970) Atomic vibrations in vitreous silica. *Discuss Faraday Soc* 50: 55–61.
41. Wang L, et al. (2018) Low-frequency vibrational modes of stable glasses. arXiv:1804.08765.
42. Schirmacher W, Ruocco G, Mazzone V (2015) Heterogeneous viscoelasticity: A combined theory of dynamic and elastic heterogeneity. *Phys Rev Lett* 115: 015901.
43. Kob W, Andersen HC (1994) Scaling behavior in the β-relaxation regime of a supercooled Lennard-Jones mixture. *Phys Rev Lett* 73:1376–1379.
44. Volpe G, Kurz L, Callegari A, Volpe G, Gigan S (2014) Speckle optical tweezers: Micromanipulation with random light fields. *Opt Express* 22:18159–18167.
45. Di Leonardo R, Ianni F, Ruocco G (2007) Computer generation of optimal holograms for optical trap arrays. *Opt Express* 15:1913.
46. Ghosh A, Chikkadi VK, Schall P, Kurchan J, Bonn D (2010) Density of states of colloidal glasses. *Phys Rev Lett* 104:248305.
47. Grigera TS, Parisi G (2001) Fast Monte Carlo algorithm for supercooled soft spheres. *Phys Rev E* 63:045102.
48. Rosenfeld Y, Tarazona P (1998) Density functional theory and the asymptotic high density expansion of the free energy of classical solids and fluids. *Mol Phys* 95:141–150.
49. Bonnans JF, Gilbert JC, Lemaréchal C, Sagastizábal CA (2006) *Numerical Optimization: Theoretical and Practical Aspects* (Springer, Berlin).
50. Lehoucq R, Maschhoff K, Sorensen D, Yang C (2008) Arpack—Arnoldi package. Available at www.caam.rice.edu/software/ARPACK/. Accessed August 2, 2018.